CITATION: V. Pejović, E. Georgitzikis, I. Lieberman, P. E. Malinowski, P. Heremans, and D. Cheyns "New methods for spectral imaging in shortwave infrared for augmented reality applications", Proc. SPIE 12449, Optical Architectures for Displays and Sensing in Augmented, Virtual, and Mixed Reality (AR, VR, MR) IV, 1244914 (16 March 2023); https://doi.org/10.1117/12.2648844

# New Methods for Spectral Imaging in Shortwave Infrared for Augmented Reality Applications

V. Pejović[*ab], E. Georgitzikis[b], I. Lieberman[b], P. E. Malinowski[b], P. Heremans[ab], D. Cheyns[b]
[a]Department of Electrical Engineering (ESAT), KU Leuven, Kasteelpark Arenberg 10, Belgium;
[b]IMEC, Kapeldreef 75, 3001 Leuven, Belgium

## ABSTRACT

Hyperspectral and multispectral imaging enable augmented reality experience by collecting spectral information of a scene and mapping it onto a 2D image. This imaging method is especially powerful if done in short-wave infrared (SWIR) because of the unique spectral fingerprints of many molecules found in this region of the spectrum. Despite its high potential, this technology has not been widely adopted due to the high price of standard SWIR cameras. Recently, image sensors based on colloidal quantum dot thin films have gained a lot of attention due to their potential to enable affordable and high-resolution SWIR imaging. In this work, we present the latest results of our efforts to leverage imec's thin-film SWIR imaging platform for spectral imaging. We present the measurement results of our multispectral photodetectors, as well as the results of optical simulations demonstrating new concepts for light filtering in the SWIR region, compatible with the thin-film technology.

**Keywords:** SWIR, hyperspectral imaging, multispectral imaging, thin-film photodetectors, quantum dots

## 1. INTRODUCTION

Multispectral and hyperspectral (from here on just spectral) imaging are techniques used for simultaneous collection of spatial and spectral information of a scene or an object. For majority of commercial applications, trichromatic imaging in red, green, and blue (RGB) is sufficient as it matches human vision. However, when the spectrum is collected in more bands, richer information can be obtained (figure 1a), which is attractive for numerous applications in machine vision, remote sensing, medicine, and many others. Depending on the number of available bands, this technique is referred to as multispectral or hyperspectral, albeit without a clear distinction in the industry between the two. In general, hyperspectral imaging typically refers to a continuous collection of the spectrum, commonly using hundreds of bands. On the other hand, multispectral imaging uses fewer bands, and the choice depends on the application.

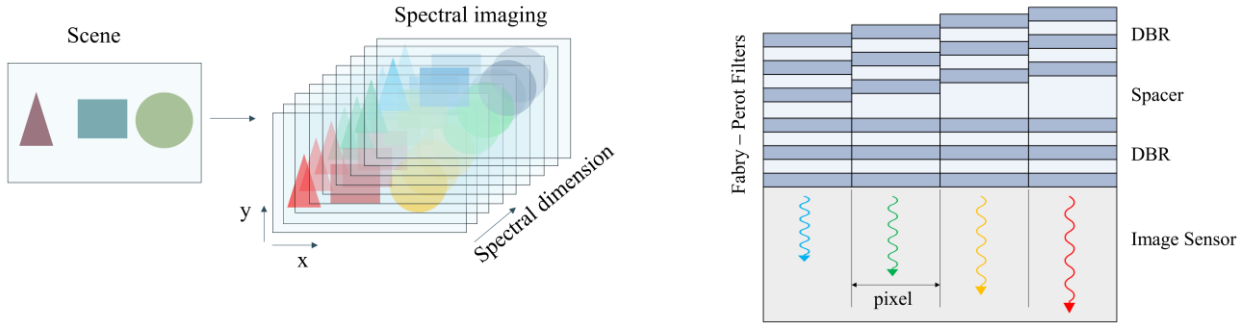


(a) (b)

Figure 1. (a) Spectral imaging provides two spatial and one spectral dimension, often referred to as (hyper)spectral data cube, (b) illustration of integrated FP optical filters on image sensors

The spectra obtained from spectral image sensors are mapped onto a 2D image and different objects can be classified and distinguished between each other based on their spectral properties i.e., constituent materials, rather than color. This approach enables augmented reality experience where a user can have real-time insights about the objects and materials

Optical Architectures for Displays and Sensing in Augmented, Virtual, and Mixed Reality (AR, VR, MR) IV,
edited by Bernard C. Kress, Christophe Peroz, Proc. of SPIE Vol. 12449, 1244914
© 2023 SPIE · 0277-786X · doi: 10.1117/12.2648844

from a scene, which are not visible by a naked eye. For example, spectral imaging can provide surgeons information about tissue composition or oxygenation during interventions.[1,2] Similarly, drivers could obtain more details about road conditions and distinguish wet from dry asphalt, observe ice formation etc.[3–5]

Optical filters based on Fabry-Perot resonant cavities are nowadays the most common approach for spectral imaging due to their compactness and compatibility with CMOS fabrication, allowing them to be integrated with image sensors on a large scale (figure 1b).[6–9] Spectral image sensors with integrated FP filters come in various configurations, such as push-broom that requires scanning of an image sensor over a scene, commonly used on industrial conveyor belts, or snapshot type that captures all the bands simultaneously, suitable for applications that require fast operation.

SWIR region (wavelength range 1 – 2.5 μm) is particularly interesting for spectral imaging since the chemistry is more 'visible' in SWIR compared to the visible or near-infrared (NIR, wavelength range 0.7 – 1 μm) part of the spectrum. Many chemical compounds such as water, proteins, lipids, fats, polymers etc., have distinct absorption features in SWIR. Moreover, due to the reduced scattering at longer wavelengths, SWIR can penetrate many materials deeper compared to visible or NIR light, providing information from below the surface. Hence, spectral imaging in SWIR is a powerful technique that combines infrared spectroscopy and imaging.

InGaAs focal plane arrays (FPAs) are the common choice for imaging in SWIR. FPAs have been traditionally used in niche applications such as defense because of their high cost. In addition, due to the hybrid integration (figure 2a), they suffer from low resolution. In order to enable spectral imaging with FPAs, FP filters need to be integrated on top of them, which further increases the integration complexity and cost,[9] making spectral imaging in SWIR reserved for low-volume applications. Moreover, for applications that require high-speed snapshot spectral imaging, division of FPA between different spectral bands degrades spatial resolution, which is particularly problematic in the case of InGaAs FPA that have large pixels (typically above 10 μm). Hence, the level of detail that can be captured with multispectral SWIR image sensors is limited.

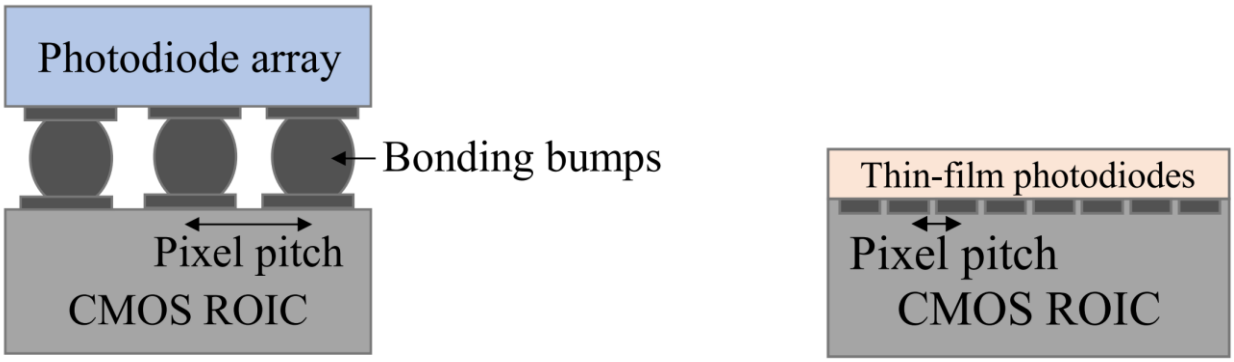


Figure 2. (a) Hybrid integration of a III-V or II-VI photodiode array to a CMOS ROIC and (b) monolithic integration of thin-film photodiodes on a CMOS ROIC.

Recently, image sensors based on thin-film absorbers such as colloidal quantum dots (CQDs) have been demonstrated as a promising alternative to conventional infrared FPAs.[10] CQDs are chemically synthesized nanocrystals with a tunable bandgap. Thanks to this feature, their absorption spectrum can be adjusted for the SWIR range. Thin-film photodiodes employing CQD absorbers can be monolithically integrated with CMOS readout integrated circuits (ROICs) (figure 2b), which opens a path for affordable and high-resolution SWIR image sensors.

Various approaches for multispectral sensing with CQD thin-film photodetectors have been demonstrated in the literature.[11–14] However, these solutions are not scalable to a large number of small pixels, which is necessary for imaging, the fabrication process becomes increasingly complicated with the increasing number of spectral bands, and the spectral resolutions is limited by the absorption profile of CQD absorbers. Here, we present the optical simulations and experimental results of multispectral thin-film photodetectors that can be integrated on CMOS ROICs for spectral imaging in SWIR with high spatial and spectral resolution.

## 2. RESULTS

CQD thin-film image sensors could, in principle, be used for spectral imaging by integrating FP filters directly on top of them. Integration of FP filters with thin-film photodetectors based on HgTe CQDs has been demonstrated by Tang et al.[15] However, the photodetectors were illuminated through the glass substrate, which is not compatible with top-illuminated image sensors. Moreover, the operation of transmission filters is affected by the back metal reflector of the CQD photodetectors, an indispensable part of the thin-film image sensor design, resulting in parasitic peaks and peak broadening.[15]

Due to the optical interference in optically thin films, photodiodes exhibit a non-uniform external quantum efficiency (EQE). Hence, if conventional optical filters were integrated on thin-film photodetectors employing CQD absorbers, the result would be that EQE after filtering would significantly vary from band to band (figure 3). Moreover, in the regions of low EQE (destructive interference), the post-filtering EQE could drop below 10% (figure 3). Hence, we resort to a different approach to light filtering which is based on optical microcavities.

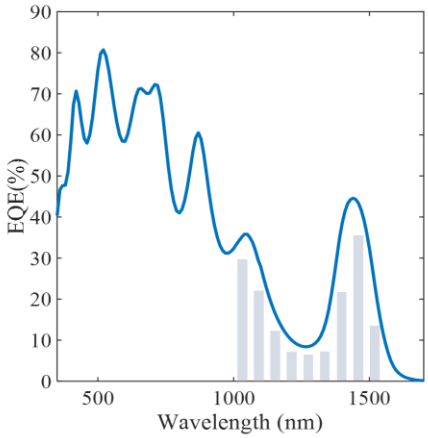


Figure 3. Measured EQE showing interference patterns with illustrated filtered bands (gray rectangles), indicating the resultant discrepancy in EQE between the bands if standard transmission FP filters were integrated on top of thin-film photodetectors.

### 2.1 Microcavity thin-film photodetectors

Instead of placing FP transmission filters in front of an absorber, in microcavity approach the absorber is placed within a FP cavity (figure 4a). Hence, the light is not absorbed after it passes through a FP cavity, but within the cavity itself. This type of photodetector is also known as a resonant cavity photodetector, commonly used with III-V materials to achieve high-speed operation for optical communications.[16] Since standard thin-film photodetectors rely on reflection from the metal back electrode for absorption enhancement, only one additional element i.e., one additional mirror, is needed to turn the standard thin-film photodetector into a microcavity configuration. For this purpose, typically a thin semi-transparent metal such as silver or gold is deposited on the illumination side as the front electrode. With the addition of a highly reflective electrode, the absorber is embedded within an optical cavity which has a filtering effect. Only light with resonant wavelengths penetrates the cavity, which is defined by the cavity's optical thickness, whereas the rest is reflected, enabling narrowband response. If the cavity length is varied by changing the thickness of any of the constituent layers of the photodetector, the resonant wavelengths can be tuned (figure 4a).

Figure 4b shows optical simulations (transfer matrix method) of a microcavity photodetector employing CQD absorber and 25 nm thick top copper reflector. By changing the length of the cavity, the position of the resonant peak can be shifted. The obtained EQE values are in the 38-53% range. Moreover, the full width at half maximum (FWHM), which defines the spectral resolution, is in the 12-17 nm range. Figure 4c shows the effect of the top reflector thickness. By increasing its thickness, the FWHM can be reduced to 10 nm, albeit at the expense of reduced EQE due to the increased losses in the metal. This tradeoff could be circumvented by employing a dielectric mirror such as distributed Bragg reflector (DBR) which would lead to a higher EQE and lower FWHM.

These simulations prove that the microcavity CQD photodetectors can be used as an effective approach for spectral imaging in SWIR with high spectral resolution. In our previous work,[17] we have demonstrated photolithographic patterning

of thin-film CQD photodiodes into 5 μm pixels in our 200 mm CMOS foundry. This capability allows us to fabricate high-resolution spectral image sensors by patterning optical microcavities with a variable thickness.

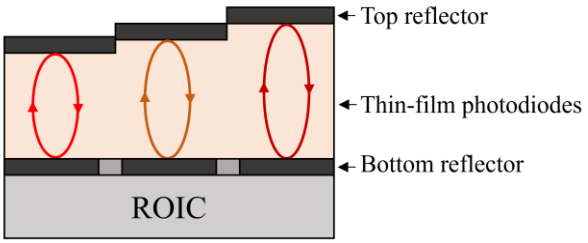


(a)

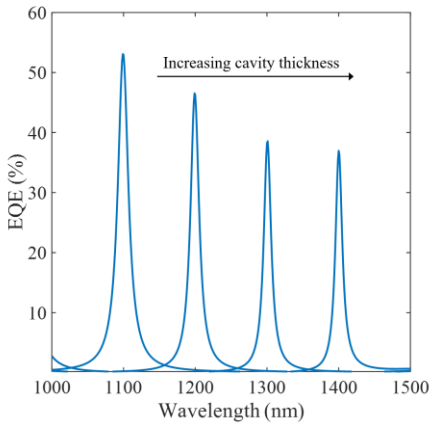


(b)

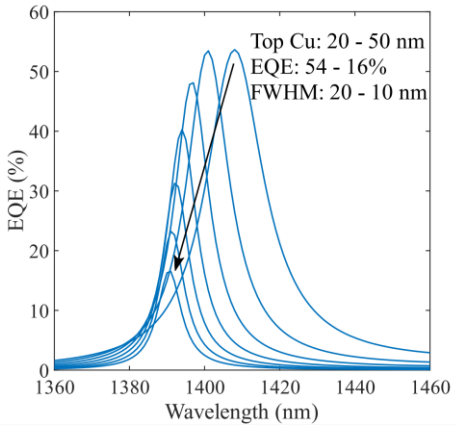


(c)

Figure 4. (a) Illustration of microcavity photodetectors with a variable thickness on top of a CMOS ROIC for spectral imaging, (b) EQE of simulated microcavity photodetectors employing PbS CQD absorbers with 25 nm thick top reflector and (c) simulated EQE of a microcavity photodetector for different thickness of the top copper semi-transparent mirror.

### 2.2 Stacked photodiodes for dual-band visible-infrared imaging

In order to enable augmented reality applications with spectral imaging, it is necessary to superimpose infrared spectral information over a standard RGB visible image. In our previous work,[18] we demonstrated dual-band sensing with thin-film photodetectors by stacking two photodiodes with different absorption spectra. By doing time division between the two photodiodes, two different spectral channels can be accessed, without compromising the spatial resolution. The top (front) photodiodes can be used to capture a visible image, and spectral infrared information captured by the bottom (back) photodiodes can be directly mapped to the corresponding RGB pixels (figure 5).

The photodetectors we demonstrated in the previous work were fabricated on glass substrates. For imaging purposes, it is necessary to develop top-illuminated photodetectors for integration on ROICs. Here, we discuss the design of dual-band stacked photodetectors on silicon substrates in a top-illuminated configuration and show the characterization results.

We fabricated dual-band photodetectors on silicon substrates with reflective TiN electrodes. The stack consists of a bottom (back) PbS CQD photodiode that absorbs longer wavelength and a top (front) CQD photodiode that absorbs shorter wavelengths, corresponding to larger and smaller CQDs, respectively. The two pn junctions were fabricated by controlling the doping type of CQD films via the surface chemistry.[18] $TiO_2$ films were used as electron transport layers, organic polymer PolyTPD as hole transport layer, and a semi-transparent ITO electrode was deposited on top of the stack (figure 6a).

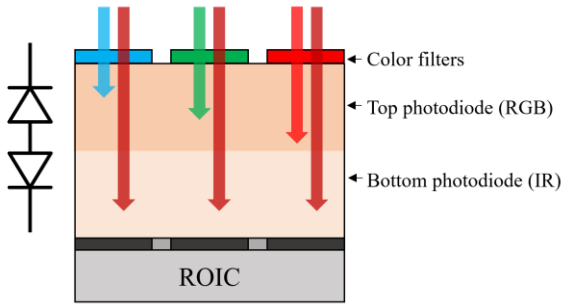


Figure 5. Combined RGB and infrared imaging by dual-band thin-film photodetectors

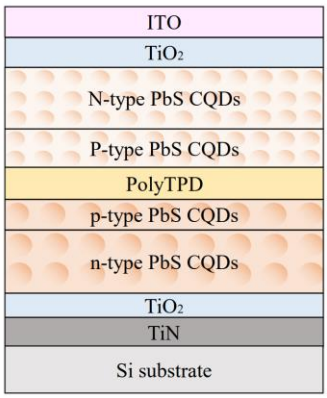


(a)

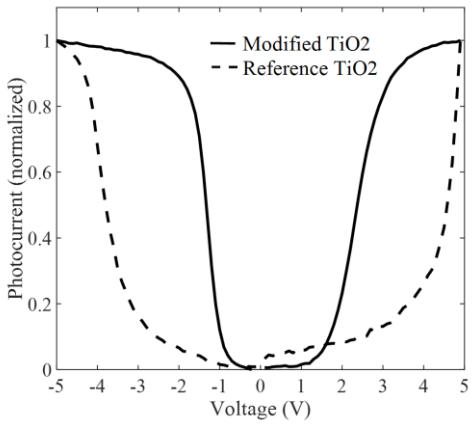


(b)

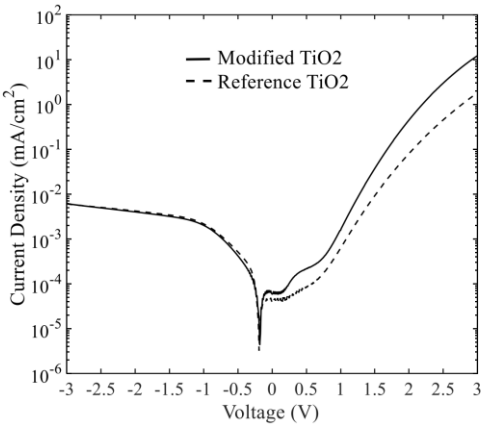


(c)

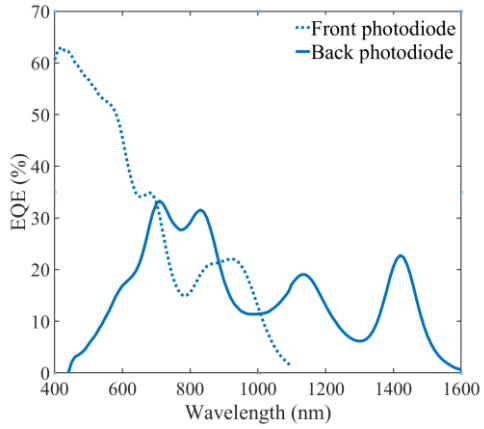


(d)

Figure 6. Top-illuminated dual-band photodetector: (a) stack illustration, (b) normalized measured photocurrent versus voltage, (c) measured IV curves of single top-illuminated photodiodes with TiN bottom electrodes employing different $TiO_2$ electron transport layers and (d) measured EQE spectra of the two photodiodes.

The two photodiodes in the stack are connected in series and it is necessary that photo-generated charge carriers can flow in both directions unhindered. We observed that a high voltage bias in excess of 5 V (absolute) was needed to saturate the photocurrent of both photodiodes in our first design (figure 6b, dashed curve), which is undesirable for the operation of

image sensors. We posited that the high resistivity could originate from the decreased carrier injection efficiency at the electrodes, both at bottom TiN and top ITO electrodes. To test this hypothesis, we fabricated standard single top-illuminated photodiodes with TiN electrodes and different $TiO_2$ transport layers. Whereas the original photodiode had a 20 nm thick $TiO_2$ film, the optimized photodiode had a modified 10 nm thick $TiO_2$ film, deposited under two times lower oxygen flow, which is expected to lead to a lower series resistance. The measured IV curves shown in figure 6c show that the modified $TiO_2$ indeed reduces the resistance, judging by the higher forward current. Then, we applied the modified $TiO_2$ in the dual-band stack, and the obtained results prove that the hypothesis was correct. The onset of photocurrent versus voltage curve shifted by approximately 2 V towards the 0 V point (figure 6b, solid curve), both on the positive (front photodiode) and negative (back photodiode) side of the voltage axis. Two EQE curves were measured (figure 6d), one under positive and the other under negative voltage bias, demonstrating the dual-band sensing functionality. The obtained EQE in visible was in the range of 40-60%, and up to 22% in SWIR. If the bottom photodiodes are placed within FP cavities with variable thicknesses, then the spectral information can be captured and the spectral crosstalk between the two channels is reduced.[18]

## 3. CONCLUSION

In this paper we presented our approach to enable augmented reality imaging by combining RGB imaging with spectrally resolved SWIR imaging. We showed the optical simulations of microcavity photodetectors based on thin-film CQD absorbers, proving that this approach can provide a high spectral resolution in combination with a high sensitivity. Furthermore, we presented the characterization results of top-illuminated dual-band photodetectors for integration on CMOS ROICs for simultaneous visible-infrared imaging.

## REFERENCES


[1] Chin, M. S., "Hyperspectral imaging for early detection of oxygenation and perfusion changes in irradiated skin," J Biomed Opt **17**(2) (2012).

[2] Yahata, A., Takemura, H., Takamatsu, T., Yokota, H., Iwanami, R., Umezawa, M., Okubo, K., Soga, K., Mitsui, T., Kadota, T., Kuwata, T. and Ikematsu, H., "Wavelength Selection of Near-Infrared Hyperspectral Imaging for Gastric Cancer Detection," ICIIBMS 2021 - 6th International Conference on Intelligent Informatics and Biomedical Sciences (2021).

[3] Bertozzi, M., Fedriga, R. I. and D'Ambrosio, C., "Adverse driving conditions alert: Investigations on the SWIR bandwidth for road status monitoring," Lecture Notes in Computer Science (including subseries Lecture Notes in Artificial Intelligence and Lecture Notes in Bioinformatics) **8156 LNCS**(PART 1) (2013).

[4] Casselgren, J., Rosendahl, S., Sjödahl, M. and Jonsson, P., "Road condition analysis using NIR illumination and compensating for surrounding light," Opt Lasers Eng **77** (2016).

[5] Ma, X. and Ruan, C., "Method for black ice detection on roads using tri-wavelength backscattering measurements," Appl Opt **59**(24) (2020).

[6] Geelen, B., Tack, N. and Lambrechts, A., "A snapshot multispectral imager with integrated tiled filters and optical duplication," Advanced Fabrication Technologies for Micro/Nano Optics and Photonics VI **8613** (2013).

[7] Geelen, B., Tack, N. and Lambrechts, A., "A compact snapshot multispectral imager with a monolithically integrated per-pixel filter mosaic," Advanced Fabrication Technologies for Micro/Nano Optics and Photonics VII **8974** (2014).

[8] Tack, N., Lambrechts, A., Soussan, P. and Haspeslagh, L., "A compact, high-speed, and low-cost hyperspectral imager," Silicon Photonics VII **8266** (2012).

[9] Gonzalez, P., Pichette, J., Vereecke, B., Masschelein, B., Lambrechts, A., Krasovitski, L. and Bikov, L., "An extremely compact and high-speed line-scan hyperspectral imager covering the SWIR range," 2018.

[10] Pejovic, V., Georgitzikis, E., Lee, J., Lieberman, I., Cheyns, D., Heremans, P. and Malinowski, P. E., "Infrared Colloidal Quantum Dot Image Sensors," IEEE Trans Electron Devices, 1–11 (2021).

[11] Mahmoud, N., Walravens, W., Petit, R., van Daele, M., Detavernier, C., Hens, Z. and Roelkens, G., "Multi-spectral SWIR PbS Quantum dot pixels realized using transfer printing," Optics InfoBase Conference Papers **Part F131-IPRSN 2019** (2019).

[12] Zhang, S., Chen, M., Mu, G., Li, J., Hao, Q. and Tang, X., "Spray-Stencil Lithography Enabled Large-Scale Fabrication of Multispectral Colloidal Quantum-Dot Infrared Detectors," Adv Mater Technol (2021).

[13] Kim, J., Kwon, S. M., Kang, Y. K., Kim, Y. H., Lee, M. J., Han, K., Facchetti, A., Kim, M. G. and Park, S. K., "A skin-like two-dimensionally pixelized full-color quantum dot photodetector," Sci Adv **5**(11) (2019).
[14] Kim, J., Jo, C., Kim, M. G., Park, G. S., Marks, T. J., Facchetti, A. and Park, S. K., "Vertically Stacked Full Color Quantum Dots Phototransistor Arrays for High-Resolution and Enhanced Color-Selective Imaging," Advanced Materials **34**(2) (2022).
[15] Tang, X., Ackerman, M. M. and Guyot-Sionnest, P., "Acquisition of Hyperspectral Data with Colloidal Quantum Dots," Laser Photon Rev **13**(11) (2019).
[16] Tung, H. H. and Lee, C. P., "Design of a resonant-cavity-enhanced photodetector for high-speed applications," IEEE J Quantum Electron **33**(5) (1997).
[17] Li, Y., Karve, G., Malinowski, P. E., Kim, J. H., Georgitzikis, E., Pejovic, V., Lim, M. J., Hagelsieb, L. M., Puybaret, R., Lieberman, I., Lee, J., Cheyns, D., Heremans, P., Osman, H. and Tezcan, D. S., "Wafer Level Pixelation of Colloidal Quantum Dot Image Sensors," Digest of Technical Papers - Symposium on VLSI Technology **2022-June**, 349–350, Institute of Electrical and Electronics Engineers Inc. (2022).
[18] Pejović, V., Georgitzikis, E., Lieberman, I., Malinowski, P. E., Heremans, P. and Cheyns, D., "Photodetectors Based on Lead Sulfide Quantum Dot and Organic Absorbers for Multispectral Sensing in the Visible to Short-Wave Infrared Range," Adv Funct Mater **32**(28) (2022).